Preliminary Investigation of u-Channel π^0 and DVCS in KaonLT

DEX YADLOWSKI

STUDENT ID: 200535962

University of Regina

August 2026

Abstract

The KaonLT experiment, conducted at Jefferson Lab Hall C, aims to further understand the structure of hadrons by studying Deep Exclusive Reactions. Two key Deep Exclusive Reactions are π^0 Deep Exclusive Meson Production (DEMP) and Deeply Virtual Compton Scattering (DVCS), the latter of which being particularly useful in understanding the quark/gluon distribution within the proton. KaonLT has collected data in Hall C using the two movable magnetic spectrometers that may show evidence of DVCS in the u-channel, but in order to determine if the quality of the data is sufficient, a variety of systematic studies must be performed.

First, the process of Event Selection is performed to separate the π^0 and DVCS reactions from other data. The cut data is then compared to the predictions from the Hall C Monte Carlo package (SIMC). The offset that aligns the data with the π^0 and DVCS SIMC predictions is then determined using χ^2 minimization techniques. Finally, the plot of missing mass squared is used to determine the scaling factors that fit the SIMC predictions to the data, which is used to scale them to the data and visually compare them to the data for several other variables in what is called the Kinematic Shape Study. The objective of this study is to determine if the sum of π^0 and DVCS fits the data better than just π^0, and to search for kinematic variables that could potentially resolve DVCS from π^0.

The Kinematic Shape Study was not conclusive in finding evidence of DVCS in the KaonLT data, but it did reveal issues with the DVCS SIMC cross-section models that, if corrected, would improve further studies.

The DVCS SIMC is also used to determine which of the KaonLT datasets are feasible to measure DVCS by using knowledge of what is accepted by the spectrometers. Finally, this work provides estimates of the rate of π^0/DVCS data collection, which lays a foundation for what is to be expected in future π^0 and DVCS experiments.

Acknowledgments

Thank you to Dr. Garth Huber for supervising this project and to Alicia Postuma for her mentorship and for assisting me in calculating the rate estimates and the yields. I would also like to thank Abdenacer Hamdi, Nathan Heinrich, Muhammad Junaid, Nermin Kamal, and the rest of the KaonLT/PionLT collaboration for their advice and support throughout this project. Thank you as well to NSERC for the USRA and for providing me the opportunity to contribute to this research.

Contents

List of Figures

List of Tables

1 Introduction

1.1 Particle Physics

The objective of particle physics is to better understand the building blocks of nature itself. Protons and neutrons, which make up the nuclei of atomic matter, and pions and kaons, which bind the nuclei together, are composed of fundamental point-like particles called quarks and gluons. All particles composed of quarks and gluons are classified as hadrons, and the proton is further classified as a baryon because it contains three valence quarks (uud). Particles composed of a quark and an anti quark, such as pions and kaons, are classified as mesons. Interactions between quarks and gluons are mediated by one of the four fundamental forces of nature, the strong force, which is described by the theory of Quantum Chromodynamics (QCD). The study of different reactions involving hadrons is one way to gain a better understanding of the nature of the strong force [1].

1.2 Deep Exclusive Reactions

At Jefferson Lab, Deep Exclusive Reactions are studied using high luminosity electron beams and high-quality detectors. An exclusive reaction is one where the energy and momentum of all involved particles is either measured or uniquely reconstructed, and a deep reaction is one at a high momentum transfer in which the underlying quark-gluon nature of matter is observed. In an example of a Deep Exclusive Reaction, Deep Exclusive Meson Production (DEMP), an electron e scatters off a target particle, in this case a proton p, via the exchange of a virtual photon γ^* and produces a meson and a baryon. If a proton is taken to be the baryon and a π^0 is taken to be the meson, then the reaction is written as $p + e^- \rightarrow e^- + p + \pi^0$. π^0 DEMP is a key reaction in understanding underlying quark/gluon dynamics and nuclear matter structure.

The four-momentum of a particle is a four-dimensional vector that contains one dimension of energy and three dimensions of momentum. In this experiment, there are two important reaction "channels" that are based on the four-momentum transfer between particles: the t-channel and the u-channel. The names of the channels come from the Mandelstam variables t and u, where $t = (p_{\gamma^*} - p_{meson})^2$ is the four-momentum transfer of the virtual photon to the produced meson, and $u = (p_{\gamma^*} - p_{baryon})^2$ is the four-momentum transfer of the virtual photon to the produced baryon. In the t-channel, the magnitude of t is minimized and the meson carries the majority of the momentum and travels forward (in the center of mass frame) to be detected by spectrometers, while the baryon travels backward and is identified using conservation laws. In the u-channel, conversely, u is such that the baryon travels forward and the meson travels backward [2].

Another key Deep Exclusive Reaction is $p + e^- \to e^- + p + \gamma$, known as Deeply Virtual Compton Scattering (DVCS). DVCS is like DEMP, but instead of a meson being produced, a photon is produced. DVCS is considered a "golden channel" because competing processes that obscure the quark and gluon information are highly suppressed [3]. t-channel DVCS has been extremely useful in understanding the quark/gluon distribution within the proton, but u-channel DVCS has never before been observed. It is expected that u-channel DVCS will be high impact work, and it will provide novel information on baryon number distribution in the proton [4].

1.3 This Work

This work examines data collected during the KaonLT experiment at Jefferson Lab Hall C for potential evidence of DVCS in the u-channel. The three important KaonLT kinematic settings for this experiment are $Q^2 = -(p_e - p_{e'})^2$, the photon virtuality, $W = \sqrt{m_p^2 + 2m_p(E_e - E_{e'}) - Q^2}$, the center of mass energy, and $\epsilon = \left[1 + 2\frac{(E_e - E_{e'})^2 + Q^2}{Q^2}\tan^2(\frac{\theta_{e'}}{2})\right]^{-1}$ the virtual photon polarization. ϵ, in the datasets examined, can be high or low. Additionally, the spectrometers can be placed at different angles from the beam line to measure a greater angular coverage, which leads to the data being further organized into SHMS left, center and right (see Section 2.2).

It was found that the strongest evidence of potential u-channel DVCS is at settings of $Q^2 = 3.0$ GeV^2 and $W = 3.14$ GeV, with the SHMS at the center angle, and at low ϵ, with beam energy $E_e = 8.2$ GeV.

To determine if DVCS was measured, a variety of studies have been conducted. First, various cuts are applied to the collected data in order to select events from the reactions $p + e^- \rightarrow e^- + p + \pi^0$ (π^0 DEMP) and $p + e^- \rightarrow e^- + p + \gamma$ (DVCS) (Section 3.1). Then, the square of the missing mass in the data is compared to the predictions of the π^0 and DVCS Hall C Monte Carlo simulation (SIMC). SIMC can simulate experimental acceptance and effects of the target and detectors to predict various reactions [5]. The missing mass squared is then used to find the offset that appropriately aligns the data with the predictions of SIMC, which allows the extraction of the factors that scale them to the data (Section 3.2). Finally, the π^0 and DVCS simulated distributions can be scaled to the data to visually compare various other kinematic variables (Section 4.1). If the DVCS prediction is significantly different than that of the π^0, and it accurately describes the data, then it may indicate that DVCS has been measured and that it can be separated from π^0.

Additionally, this work investigates the feasibility of making measurements of datasets with different Q^2 and W settings using the DVCS SIMC (Section 4.2), and it provides estimates for the event rate of π^0/DVCS data collection using integration and dimensional analysis techniques (Section 4.3).

2 Experiment

The KaonLT experiment is conducted in Jefferson Lab Hall C, located in Newport News, Virginia. The main research facility of Jefferson Lab is the Continuous Electron Beam Accelerator Facility (CEBAF), which consists of two linear accelerators and arc magnets that bend the electron beam between accelerators (Figure 2.1). The electron beam can pass through the linear accelerators multiple times, gaining energy on each pass (up to 12 GeV), until it is directed into Hall C at the switch yard. The beam then travels down the beam line into the target, and the scattered particles travel into the two spectrometers [5, 6].

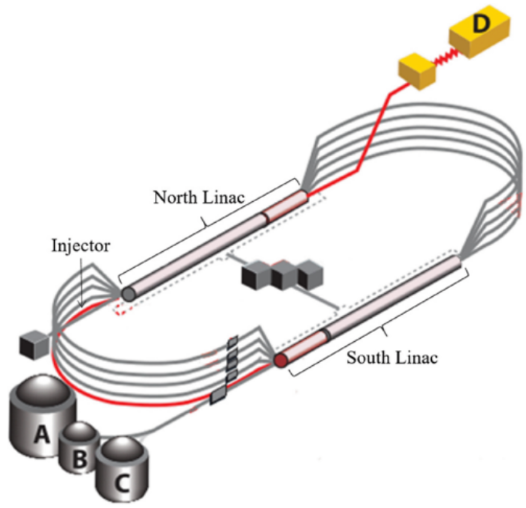

Figure 2.1: The Jefferson Lab accelerator facility. The electron beam is first accelerated by the injector into the North Linac. Arc magnets are used to bend the beam from the North Linac to the South Linac. Each pass through the linear accelerators increases the beam energy. After the desired number of passes, the beam is directed into Hall C [7].

2.1 Target

The electron beam interacts with the target, which, in this experiment, is cryogenic liquid hydrogen (LH_2) contained inside a cylindrical aluminum cell. There is also a solid target of aluminum that is used for the dummy subtraction (Section 3.1.3). The cryogenic and solid targets are housed in a target ladder that can be moved to select the desired target to be hit with the electron beam. The particles produced from the target scattering exit through the target window and may travel into the two spectrometers, while the un-scattered beam travels through to the "beam dump" [5].

2.2 Spectrometers and Detectors

The primary Hall C apparatus is the pair of two magnetic focusing spectrometers: the High Momentum Spectrometer (HMS) and the Super High Momentum Spectrometer (SHMS) (Figure 2.2). In this experiment, the magnetic fields are calibrated to direct positive particles (protons, pions, and kaons) into the SHMS and negative particles (primarily electrons) into the HMS [5, 6]. Additionally, only particles of a certain momentum (and mass) will be properly directed into the spectrometers, which allows more precise selection of particles. The spectrometers are also capable of rotating to different angles, which allows for a greater angular coverage.

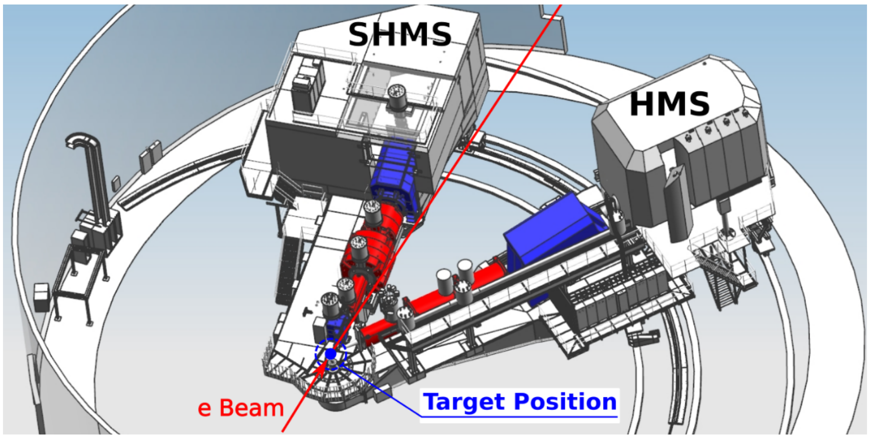

Figure 2.2: Spectrometers in Hall C. Particles are produced from the e beam scattering off the LH_2 target at the Target Position, and they travel into the SHMS and the HMS. Both spectrometers are on tracks that can be rotated [8].

Both spectrometers contain an array of detectors, including those called Cherenkov detectors, which are essential for the process of particle identification and distinguishing the detected particles from each other (see Section 3.1.1). When a charged particle in a dielectric medium travels faster than light in that medium, it produces Cherenkov radiation. Both the HMS and SHMS are equipped with gas Cherenkov detectors, where the radiation is reflected off spherical mirrors into photomultiplier tubes. The gas species and pressure affects the index of refraction, which determines if the particle will produce Cherenkov radiation. Additionally, at fixed momentum, the lighter particles will travel faster and produce Cherenkov radiation, while the heavier, slower particles will not. This allows particles to be separated by their mass in the detectors. The SHMS also has a silica aerogel Cherenkov detector, which has a higher index of refraction and allows further separation of particles [5]. The SHMS Cherenkov detectors are primarily used to distinguish protons from other positively charged particles, such as pions and kaons, and the HMS Cherenkov detector is used to distinguish electrons from other negatively charged particles.

3 Methodology

3.1 Event Selection

The π^0 and DVCS processes produce an electron and a proton that are detected by the two spectrometers. Because these are u-channel processes, the baryon (proton) travels forward to the SHMS, but the π^0 and γ travel backward and are not directly detected. In fact, because they are uncharged particles, the focusing magnets would not direct them into the spectrometers regardless of their direction of travel. As a result, the π^0 and γ are studied using conservation of energy and momentum, from what is known of the detected electron and proton.

To select the appropriate events, many specific cuts are applied to the data. The data is cut to ensure that an electon was detected by the HMS, and that a proton was detected by the SHMS. It is also cut to ensure that the electron and the proton arose from the same event, using the coincidence time between the HMS and SHMS signals.

3.1.1 Particle Identification

To ensure an electron is detected in the HMS, two cuts are made: the total normalized energy in the HMS electromagnetic calorimeter is cut to keep the electron peak and to remove negative hadrons, such as π^- mesons, and the number of photoelectrons measured in the HMS Cherenkov is cut for the same reason. The cuts are illustrated in Figure 3.1.

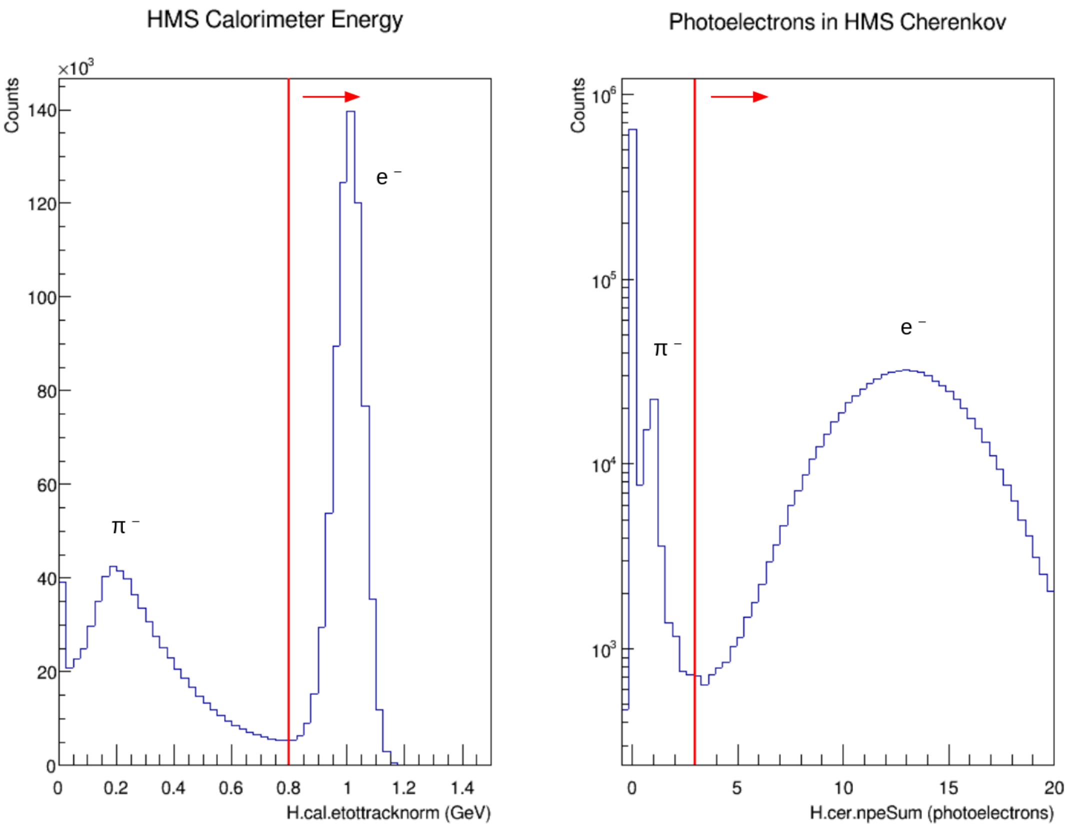

Figure 3.1: The HMS calorimeter energy (left) and the number of photoelectrons in the HMS Cherenkov (right). This data is used to ensure an electron was detected by the HMS. The red lines and arrows indicate what is kept after the cuts are applied. These plots have the Coincidence Time cut (Section 3.1.2) applied.

In order to ensure a proton is detected in the SHMS, two more cuts are made. The number of photoelectrons measured in the SHMS heavy gas Cherenkov (Figure 3.2) and the number of photoelectrons measured in the SHMS aerogel Cherenkov (Figure 3.3) are both cut to separate the proton sample from the π^+ (pions) and K^+ (kaons) that are also detected by the SHMS. In the heavy gas, pions are expected to Cherenkov while protons and kaons are not, and in the aerogel, kaons are expected to Cherenkov while protons are not.

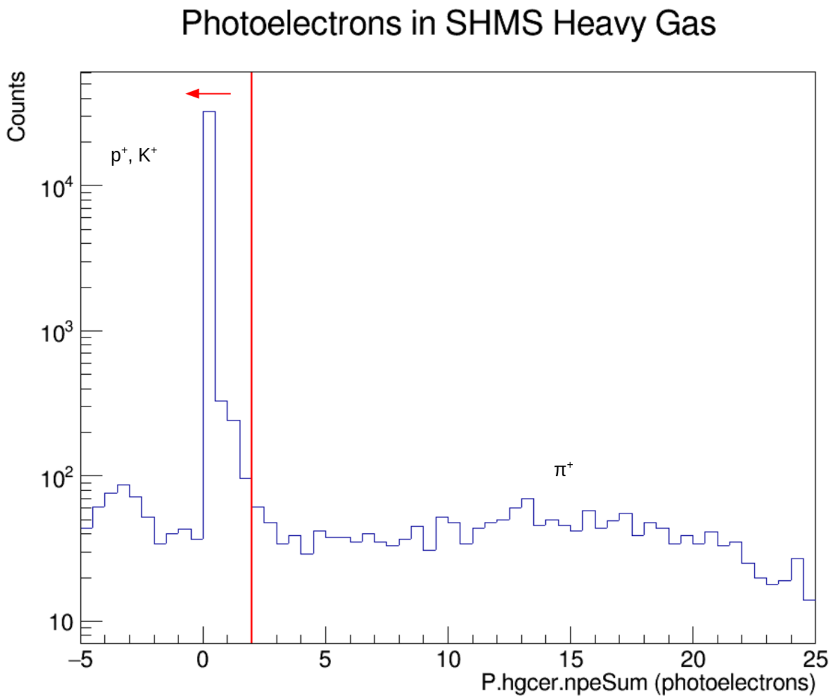

Figure 3.2: Photoelectrons in the SHMS heavy gas Cherenkov. This data is used to separate protons and kaons from pions. The red line and arrow indicate what is kept after the cut is applied. This plot has all cuts explained in this section applied.

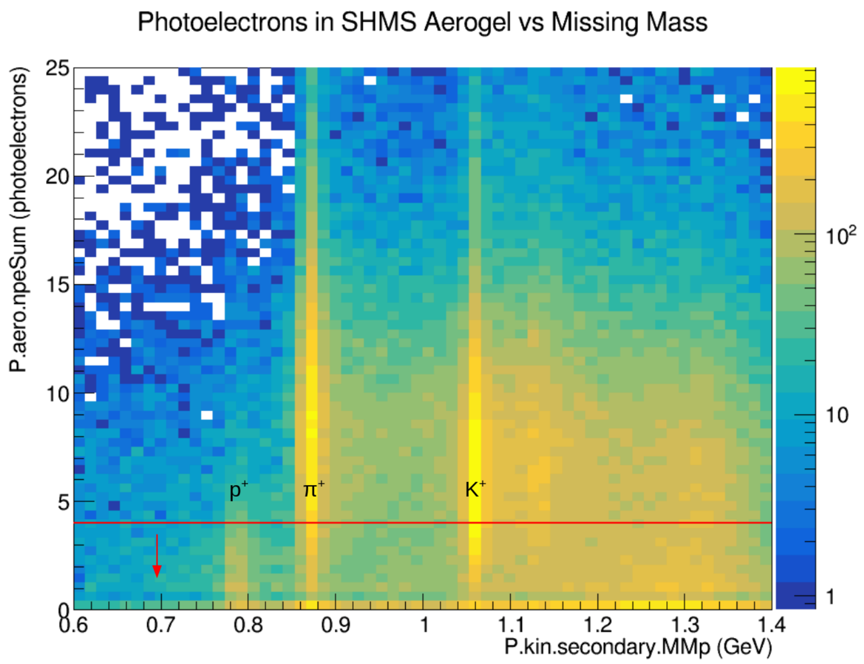

Figure 3.3: Photoelectrons in the SHMS aerogel Cherenkov plotted vs the missing mass (see Section 3.2). The faint spike at 0.79 GeV indicates that some protons interacted with materials and created secondary "knock-on" electrons that produce Cherenkov radiation in the aerogel, so they are kept in the sample. The other spikes are photoelectrons from pions and kaons, and they are mostly cut out. The red line and arrow indicate where the cut was applied. This plot has all cuts explained in this section applied.

Due to the arrangement of the spherical mirrors inside the heavy gas Cherenkov, there is an inefficient region known as the "heavy gas hole." Geometric cuts were made on the 2-dimensional plot of location of Cherenkov events inside the detector to eliminate this region. Because pions in the hole do not Cherenkov as much as they do elsewhere, removing this region is important to avoid mistaking some pions for protons.

Finally, the SHMS radiofrequency time distribution, abbreviated as RFTime, measures the time of flight of the particle between target and SHMS. It varies according to the particle's mass, at fixed momentum, and it is cut to select protons (Figure 3.4).

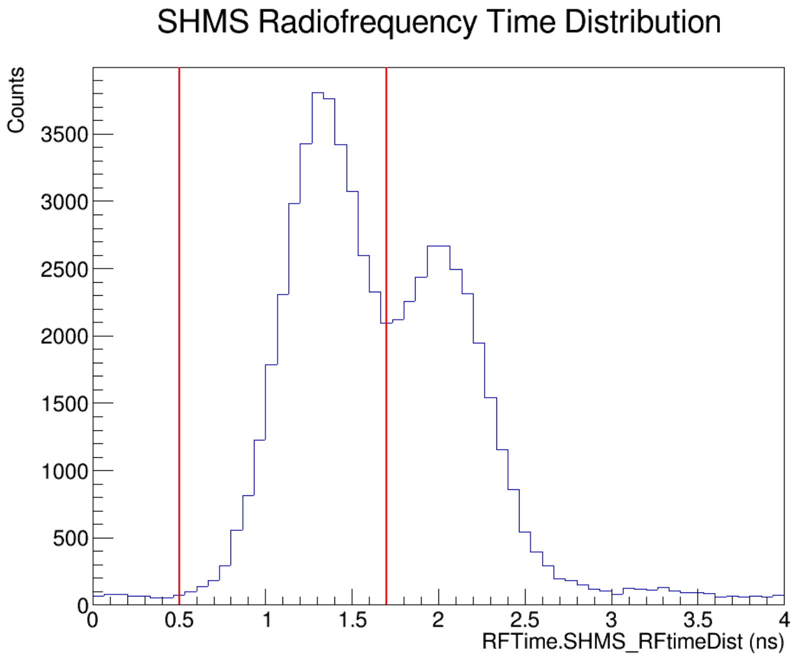

Figure 3.4: SHMS radiofrequency time distribution. Cuts are applied to select only the proton peak between the two red lines to ensure a proton is detected in the SHMS. This plot has all the previously explained cuts applied, alongisde the Coincidence Time (Section 3.1.2).

3.1.2 Coincidence Time

The coincidence time is the time between signals in the HMS and SHMS. When the electron in the HMS and the proton in the SHMS are products of the same event, it is known as a real coincidence, and if the particles are from different events, it is known as a random coincidence. An important cut is keeping only the central peak of what are called prompt events, which are made up of real and random events, and then performing a random subtraction. For a random subtraction, the average of several random peaks is calculated and subtracted from the prompt peak, leaving only real coincidence events. The cuts selecting the prompt peak are illustrated in Figure 3.5.

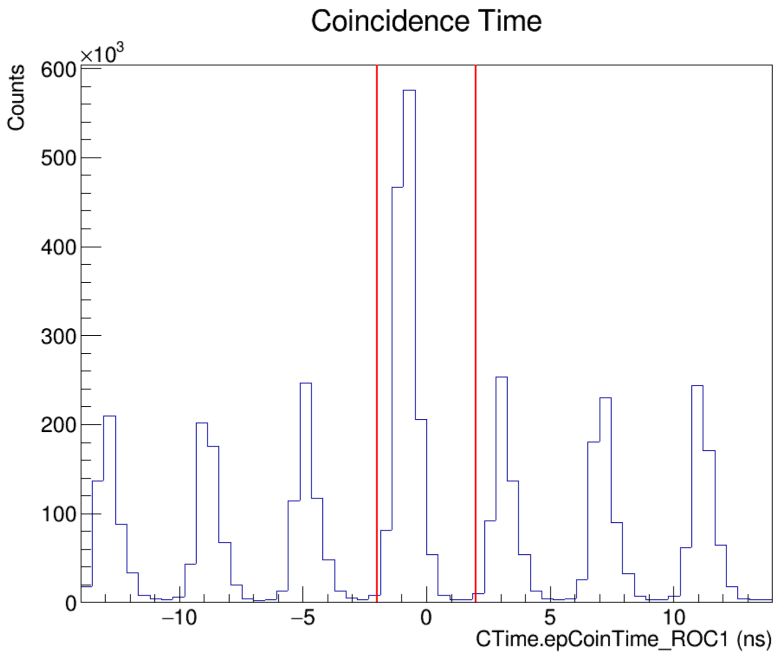

Figure 3.5: The coincidence time between the HMS and the SHMS. The central peak is from prompt coincidence events, and the small peaks on either side are from random coincidence events. Random coincidence events are eliminated from the central peak in a process called random subtraction. The red lines indicate the range of the cut around the central peak. This plot has all previously explained cuts applied.

3.1.3 Dummy Target Subtraction

Most scattering reactions occur on protons in the LH_2 target, but there are also some events from the aluminum target cell itself. To correct for these particles, a dummy target of aluminum is used to collect data that is subtracted from the LH_2 data. The yields from the LH_2 target and from the dummy target are both normalized by the effective charge of the electron beam on the target, which allows them to be properly subtracted. The dummy target is also thicker than the target cell wall, which is accounted for in the subtraction.

3.1.4 SIMC Acceptance

Aside from the data, the Hall C Monte Carlo simulation (SIMC) outputs that model the π^0 and DVCS reactions must also be modified. There are many cuts, known as acceptance cuts, that limit the events to the region of the focal plane where the optics (effects of the magnetic fields) are well understood. This is done to be confident that SIMC is properly reconstructing events. The dx/dz and dy/dz of the particle track coordinates and the δ for the HMS and SHMS, which describe the percentage difference the central spectrometer momentum and particle track momentum, are each cut to be within a specific range of values. The cuts were applied in this study, but they have already been well-established and were not re-evaluated.

3.1.5 Weight

The SIMC output events are weighted based on the cross-section of the reaction. The π^0 and DVCS have their own weights based on the respective reaction cross-sections, but there are actually two different cross-section calculation models for DVCS, which will be referred to as Model 1 and Model 2.

The study began with using DVCS Model 2, but upon investigating certain kinematic variables at high ϵ, it was found that it had strange artifacts that could not be explained. The artifacts exist at low ϵ as well, but they were not seen because they were removed by the acceptance cuts at low ϵ. A significant effort during this study was spent on examining the cross-section model of the DVCS SIMC and attempting to diagnose the issue with Model 2, but no solution has yet been found. As a result, DVCS Model 1 was used for the study instead, which did not have the artifacts present in Model 2.

However, the kinematic shape study was performed at low ϵ using Model 2 regardless of the artifacts, and there is a significant discrepancy between the two DVCS models, even with the artifacts removed by the cuts. For more discussion and a comparison of plots, see Section 4.1.1.

3.2 Missing Mass Offset

With the process of event selection complete, the majority of what remains of the data after the cuts are applied should be from the two reactions $p + e^- \rightarrow e^- + p + \pi^0$ and $p + e^- \rightarrow e^- + p + \gamma$. The next step is to plot the missing mass squared to see how π^0 and DVCS combine to form the peak in the data. The square of the missing mass is calculated using Special Relativity and conservation of energy and momentum with $m^2 = E^2 - p^2$, where E and p are the "missing" energy and momentum (the energy and momentum of the undetected π^0 or γ). The initial values are known (electron beam and proton target) and the final values are known for two of the three particles (the electron and proton that are detected in the spectrometers), so conservation laws can determine the values for the undetected particles.

The missing mass offset study is done in order to align the data with SIMC predictions. Ideally, they would already be aligned, but small offsets arise from differences in the real vs measured spectrometer position and momentum. For a given data offset, the missing mass squared SIMC predictions are fit to the data by scaling the SIMC by an amount that minimizes the χ^2 of the fit. The χ^2/NDF is then computed for several offsets, and a plot of χ^2/NDF vs offset is used to determine the optimal offset.

3.2.1 π^0/DVCS

The missing mass offset determines the relative contributions of the π^0 and DVCS SIMC because of how they scaled during the fitting to the data. This means that a greater offset increases the π^0 contribution and decreases the DVCS contribution. In Figure 3.6, there are two minima in the plot of χ^2/NDF vs offset: one where the DVCS is maximized to fill the peak in the data, and another where the π^0 is maximized. The first minimum occurs at an offset of -0.0120 GeV^2, but it is rejected because it is not expected considering other prior knowledge (u-channel DVCS is expected to be 10-100x smaller than π^0, so the fit in which DVCS comprises nearly 100% of the peak is not trusted) [9]. The second minimum, which is the global minimum, occurs at an offset of 0.0040 GeV^2. This does contain an expected ratio of DVCS to π^0.

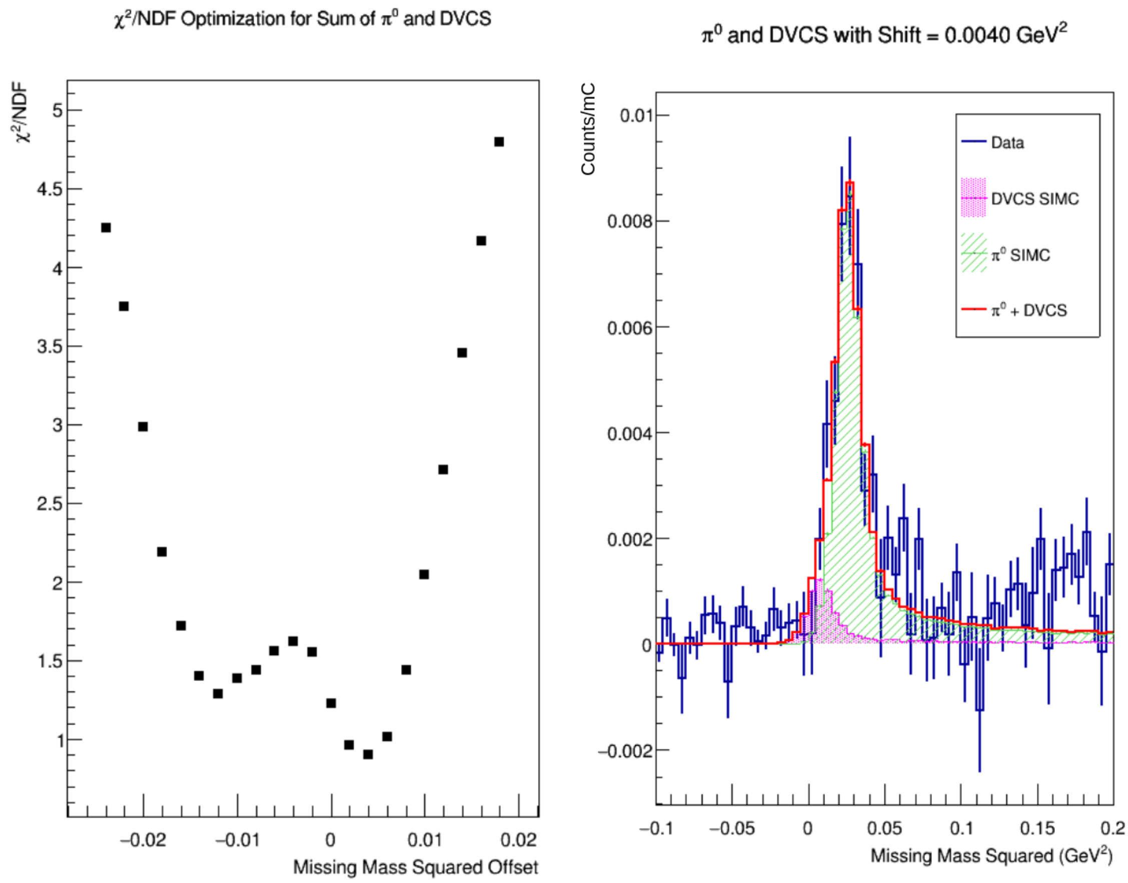

Figure 3.6: π^0/DVCS missing mass optimization. The plot of χ^2/NDF vs missing mass squared offset (left) is used to determine the optimal shift on the data to match the sum of the π^0 and DVCS SIMC predictions. Missing mass squared (right) is then plotted with the shift of the second minimum (0.0040 GeV^2) applied to the data.

3.2.2 $\pi^+ n$

A way to check the accuracy of the offset is to repeat the optimization process for other reactions, and see if the value of the offset is the same. Since the missing mass squared distribution includes several particle regions besides the π^0/DVCS region, namely, the peaks of recoil n from detected π^+ and recoil Λ^0 from detected K^+ mesons, it is expected that the offset that optimizes the π^0/DVCS region should also optimize the fit of the π^+ and K^+ SIMC outputs with their respective regions in the data.

The missing mass offset for the reaction $p + e^- \rightarrow e^- + \pi^+ + n$ can be optimized to the π^+ SIMC prediction using the same techniques and event selection, but with the particle identification cuts flipped in order to now select for pions in the SHMS. The result, shown in Figure 3.7, is that the offset with the lowest χ^2/NDF is 0.0000, or no shift. This disagrees with the precise offset predicted by the π^0/DVCS, but it is not far from the global minimum, and it is well within the region between the two minima. This discrepancy is an important source of uncertainty on the offset.

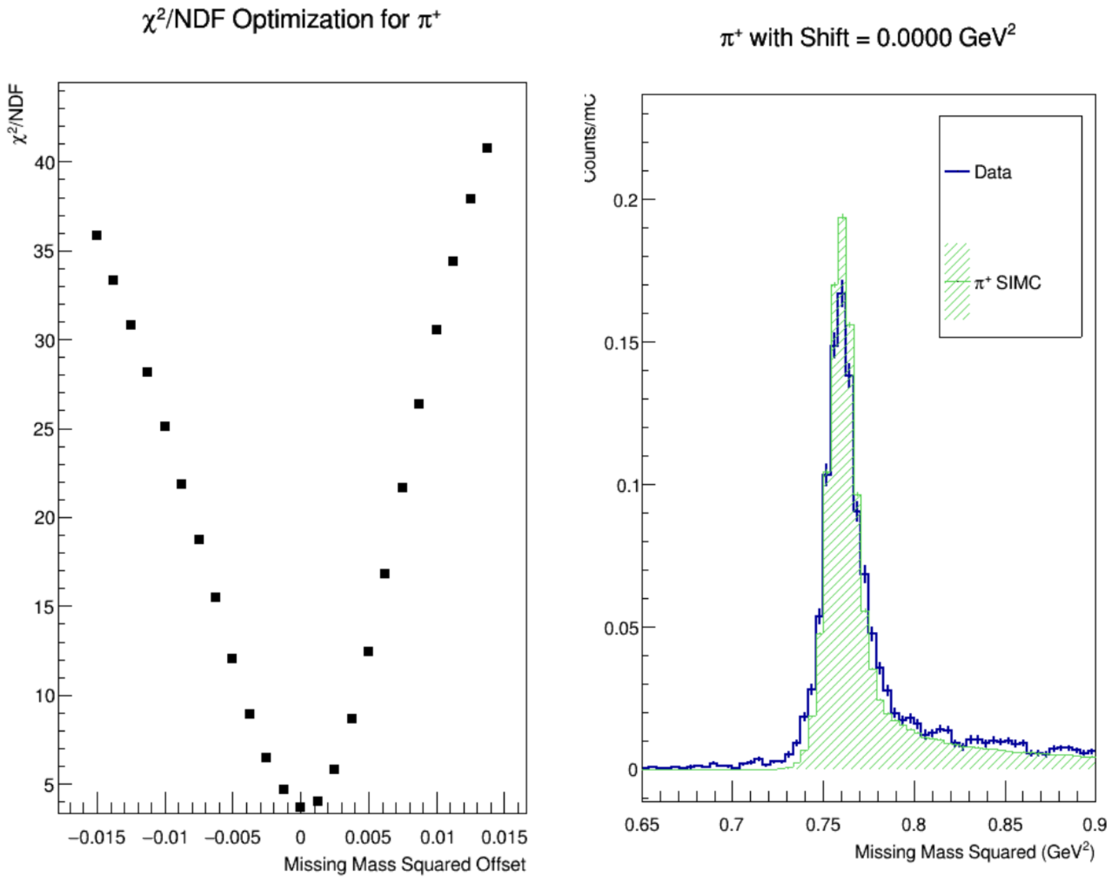

Figure 3.7: π^+ missing mass optimization. The plot of χ^2/NDF vs missing mass squared offset (left) is used to determine the optimal shift on the data to match the π^+ SIMC prediction. Missing mass squared (right) is then plotted with the shift of the minimum (0.0000 GeV^2) applied to the data.

3.2.3 $K^+\Lambda^0$

Additionally, the missing mass offset for the reaction $p + e^- \rightarrow e^- + K^+ + \Lambda^0$ is optimized to the K^+ SIMC prediction using cuts to select for K^+ mesons in the SHMS. As seen in Figure 3.8, the optimal missing mass offset for this reaction is again 0.0000, which agrees with that for the π^+.

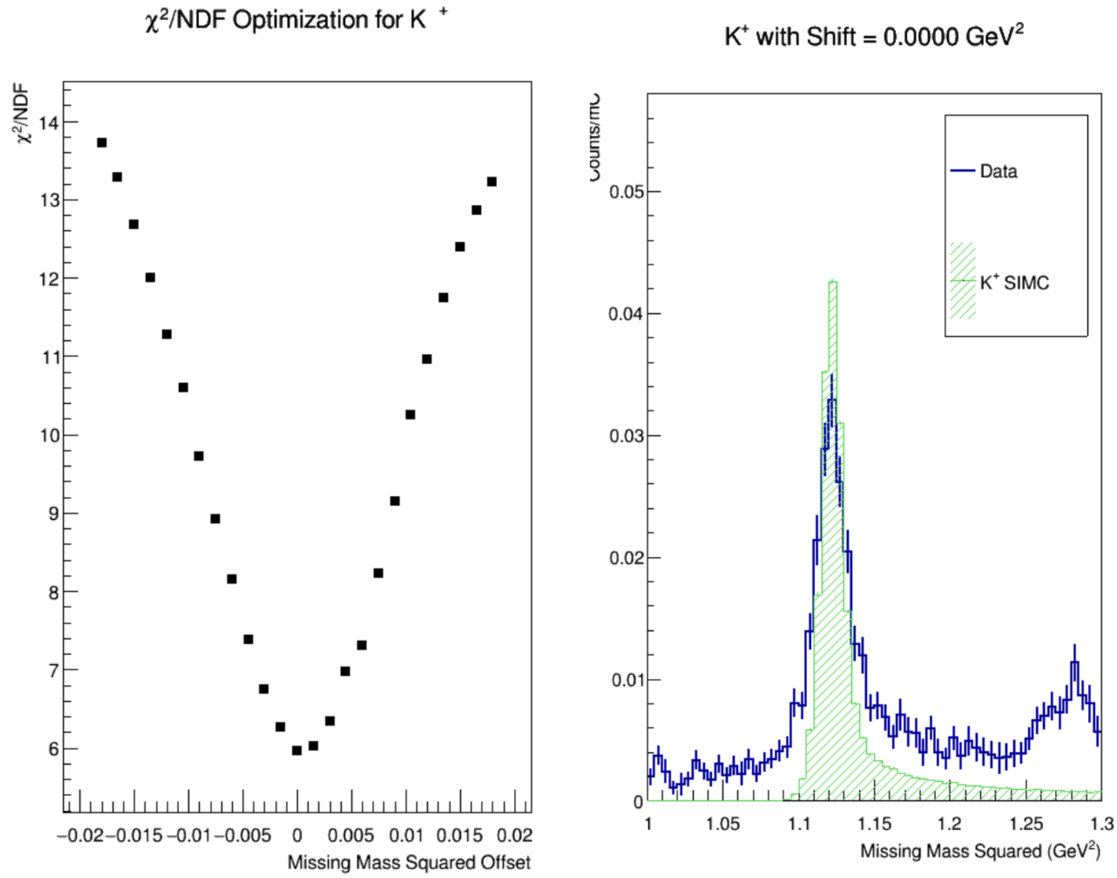

Figure 3.8: K^+ missing mass optimization. The plot of χ^2/NDF vs missing mass squared offset (left) is used to determine the optimal shift on the data to match the K^+ SIMC prediction. Missing mass squared (right) is then plotted with the shift of the minimum (0.0000 GeV^2) applied to the data.

It is important to note that the cross-section for the π^+ and K^+ reactions are significantly higher than that for π^0/DVCS, and there is much more data in these regions. Furthermore, as seen in Figure 3.7 Left and Figure 3.8 Left, the curve is narrower than that for Figure 3.6 Left. Therefore, the offsets for the π^+ and K^+ are more reliable than π^0/DVCS, especially considering that they agree with each other. The missing mass squared offset on the data is therefore set to be 0.0000 for the remainder of the study.

4 Results and Discussion

The yields of π^0 and DVCS at an offset of 0.0000 are acquired by integrating the missing mass squared plot, and they are found in Table 4.1.

	Number of Events	**Normalized Yield** (events/mC)
π^0+ DVCS	335 ± 23	0.0319 ± 0.0022
π^0	222 ± 15	0.0211 ± 0.0014
DVCS	84 ± 6	0.0080 ± 0.0005

Table 4.1: Yields of π^0 vs DVCS at an offset of 0.0000. The values are normalized by the total charge, not the effective charge, so they do not include the efficiencies required for a proper cross-section calculation.

4.1 Kinematic Shape Study

With the missing mass squared offset being 0.0000, the appropriate π^0 and DVCS SIMC scaling factors may be extracted from the missing mass squared fit (Figure 4.1). The factors are then applied to the π^0 and DVCS SIMC so that they can be visually compared to the data when plotted on the same canvas. The goal is to see if other variables show a separation of π^0 and DVCS. The data, π^0 SIMC, DVCS SIMC, and the sum of π^0 and DVCS are all plotted together. The data has all of the event selection cuts described in Section 3.1 applied, and the SIMC has the acceptance cuts (Section 3.1.4) and weight (DVCS using Model 1) applied (Section 3.1.5). Finally, one more cut is made to restrict the range of the missing mass squared over the peak so that the kinematics pertain only to the π^0/DVCS region.

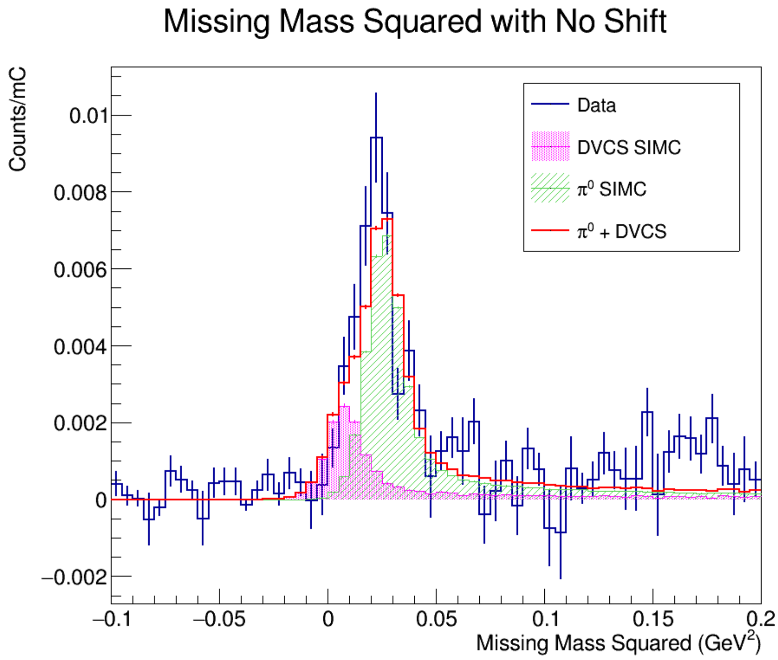

Figure 4.1: Missing mass squared for π^0 and DVCS events. The peak in the data appears to be made up of the sum of the π^0 and DVCS SIMC predictions. No shift was applied to the data, which was decided in Section 3.2. The factors that scale the π^0 and DVCS contributions are extracted from the fitting of this plot.

Data is compared to the π^0 and DVCS SIMC predictions for numerous kinematic variables, including: the total, and x-, y-, and z-components of the missing momentum in the lab coordinate frame (Figure 4.2); the missing energy (Figure 4.3); the Mandelstam variables u and t (Figure 4.4); Q^2 and W (Figure 4.5); δ of the SHMS and ϕ, which is the angle between the scattering plane and the reaction plane (Figure 4.6); and θ, which is the angle of the recoil photon with respect to the q vector, which is the momentum of the virtual photon, in the lab coordinate frame (Figure 4.7).

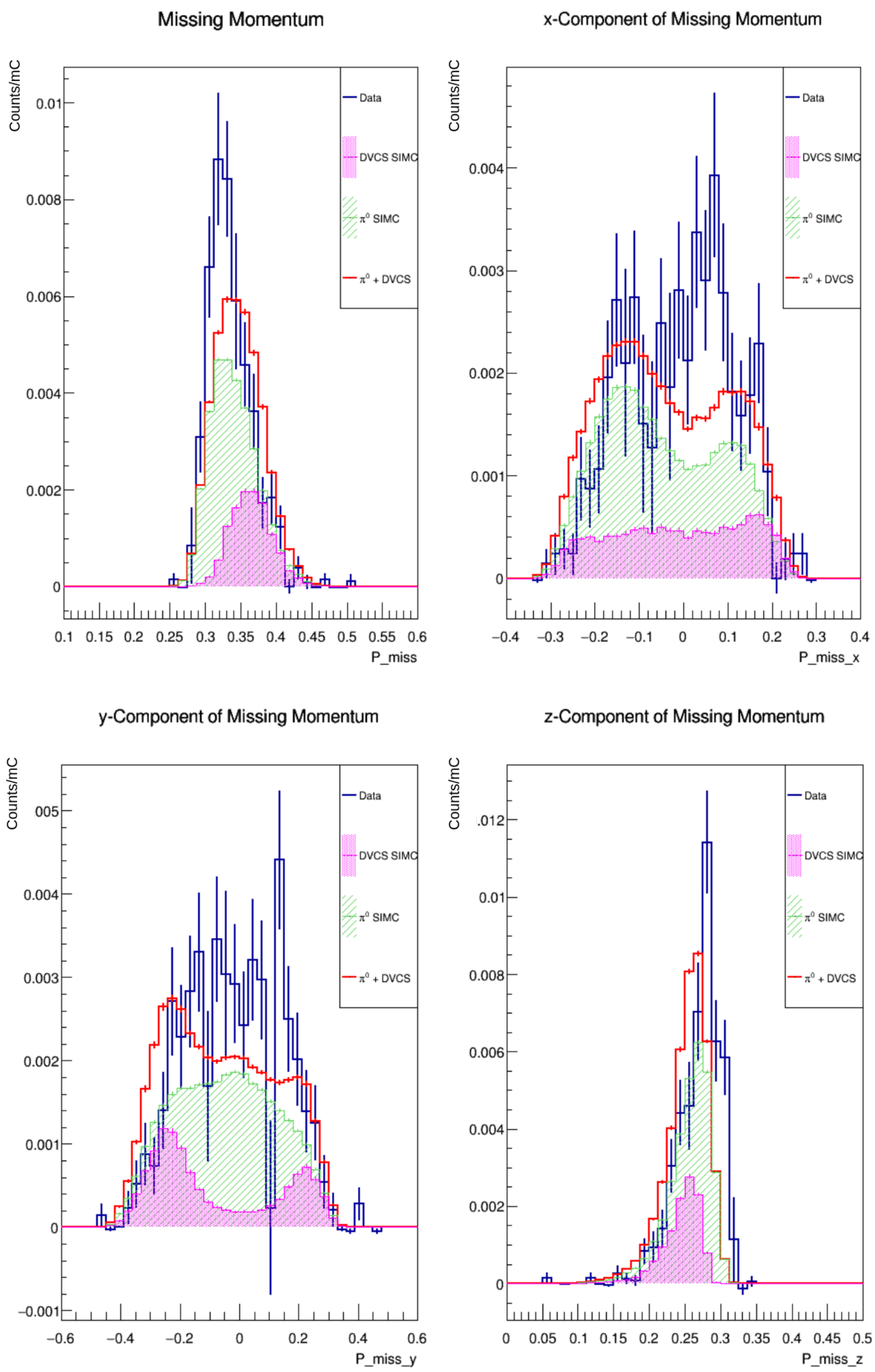

Figure 4.2: Missing momentum (total, x-, y-, and z-components) for data vs π^0 and DVCS SIMC predictions. Top Left: the DVCS peak is shifted from the π^0 peak, but not by an amount significant enough to resolve them. Top Right and Bottom Left: the π^0 and DVCS do not fit the data very nicely, but this can be due to low statistics. Bottom Right: the DVCS peak is entirely underneath the π^0 peak, and they both miss the right shoulder in the data.

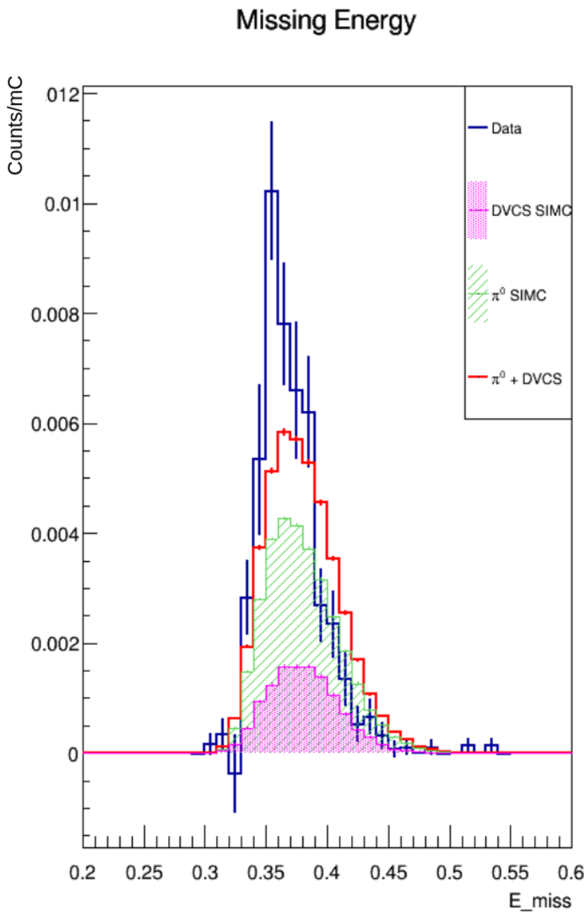

Figure 4.3: Missing energy for data vs π^0 and DVCS SIMC predictions. The DVCS peak is entirely underneath the π^0 peak, so they likely cannot be resolved from this plot.

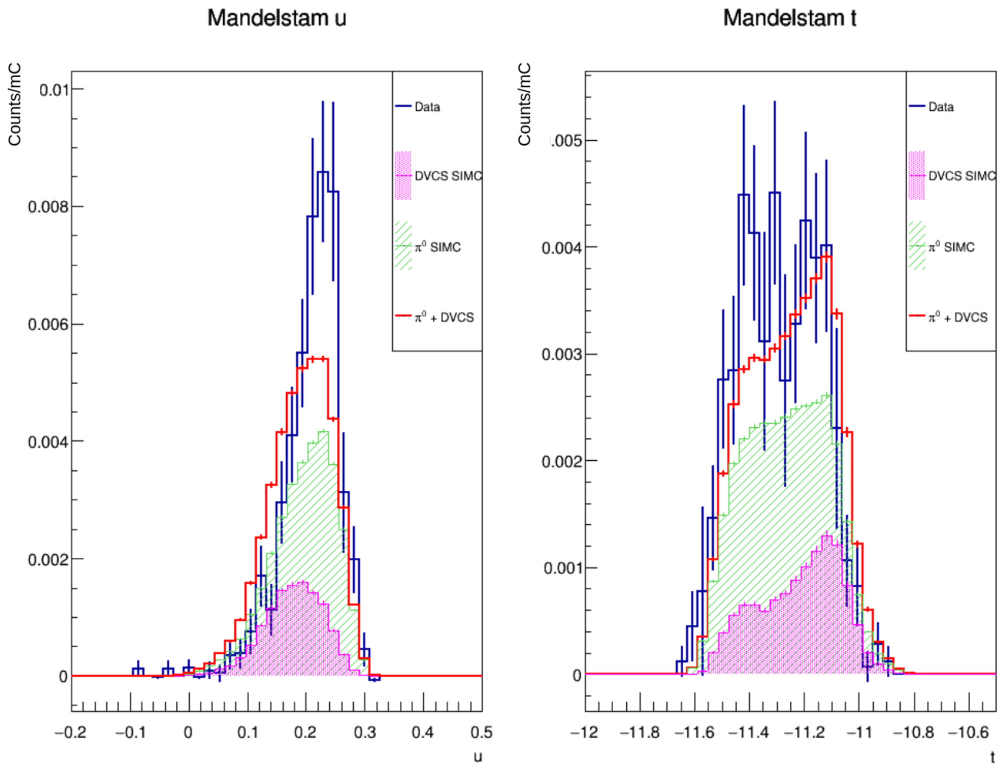

Figure 4.4: Mandelstam u and t for data vs π^0 and DVCS SIMC predictions. The DVCS peak appears similar to the π^0 peak in both plots, and they match the data reasonably well. DVCS likely cannot be resolved from π^0 for these variables.

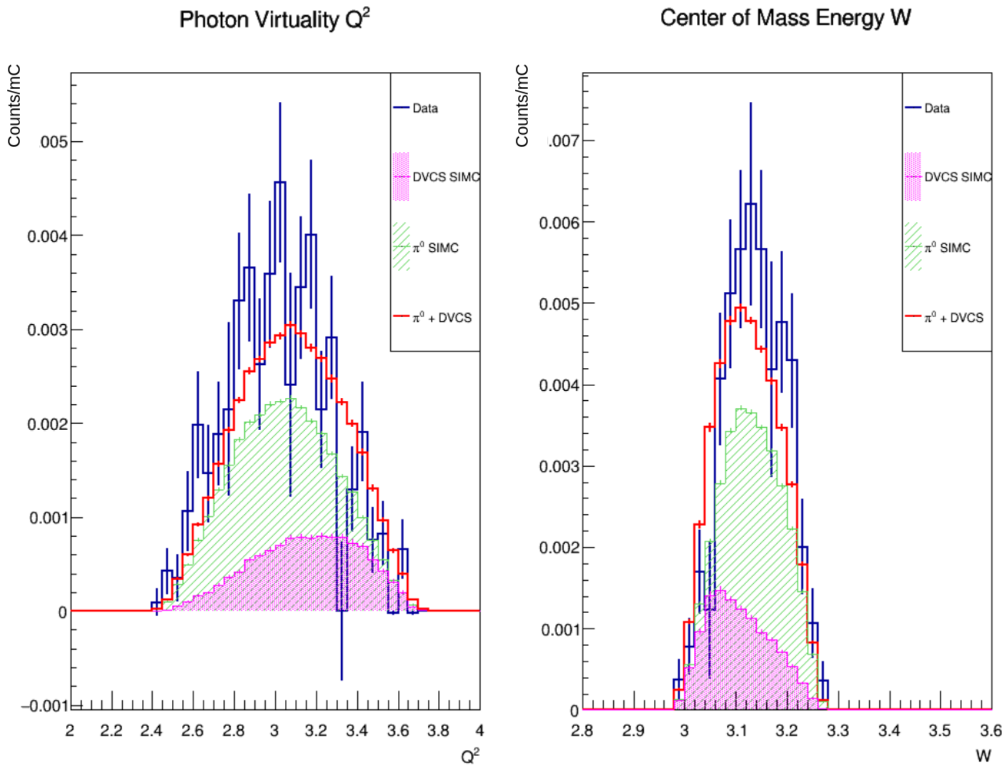

Figure 4.5: Q^2 and W for data vs π^0 and DVCS SIMC predictions. Again, the DVCS peak appears similar to the π^0 peak in both plots, and they match the data reasonably well. DVCS likely cannot be resolved from π^0 for these variables.

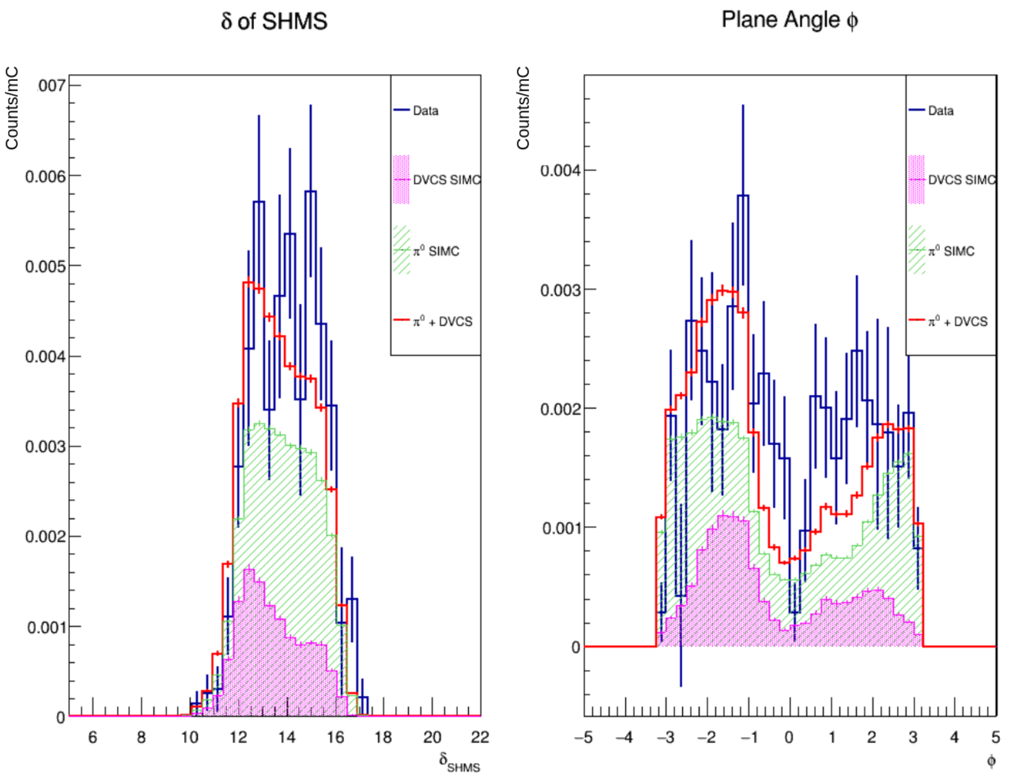

Figure 4.6: δ_{SHMS} and ϕ for data vs π^0 and DVCS SIMC predictions. Again, the DVCS peak appears similar to the π^0 peak in both plots, and they match the data reasonably well. DVCS likely cannot be resolved from π^0 for these variables either.

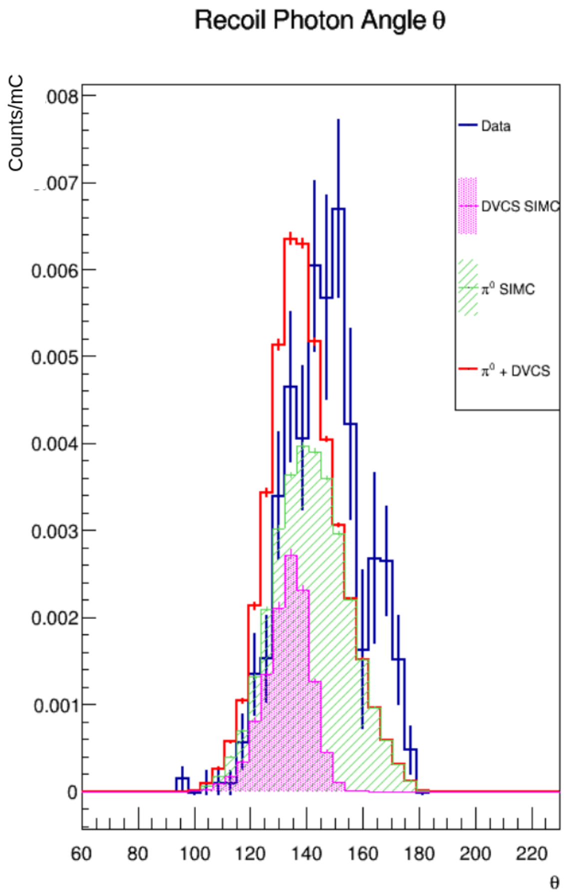

Figure 4.7: Angle of recoil photon θ for data vs π^0 and DVCS SIMC predictions. Once again, the DVCS peak appears similar to the π^0 peak, and they match the data reasonably well. The right shoulder in the data is missed by the SIMC.

In general, the DVCS SIMC predictions cannot be easily resolved from the π^0 SIMC predictions. For many of the plots, if π^0 was scaled up further and DVCS was not considered, the fit to the shape in the data would be reasonably similar, or perhaps even more accurate. The evidence of detected DVCS from the shape study alone is likely inconclusive so far.

4.1.1 DVCS Models

The plots in Section 4.1 use Model 1 for the weight in the DVCS SIMC. However, the other cross-section model, Model 2, produces different DVCS plots (see Section 3.1.5).

The kinematic shape study was repeated using DVCS Model 2, and it was found that many of the variables were nearly identical, such as the missing mass squared, while others were significantly different, such as the recoil photon angle θ. Figure 4.8 shows how θ changes when using a different DVCS model. The discrepancy between the two models of DVCS is nearly as significant as the discrepancy between the π^0 and DVCS SIMC predictions, which indicates that the kinematic shape study may not be the best way to reasonably separate π^0 from DVCS, at least until there is more confidence on the SIMC models.

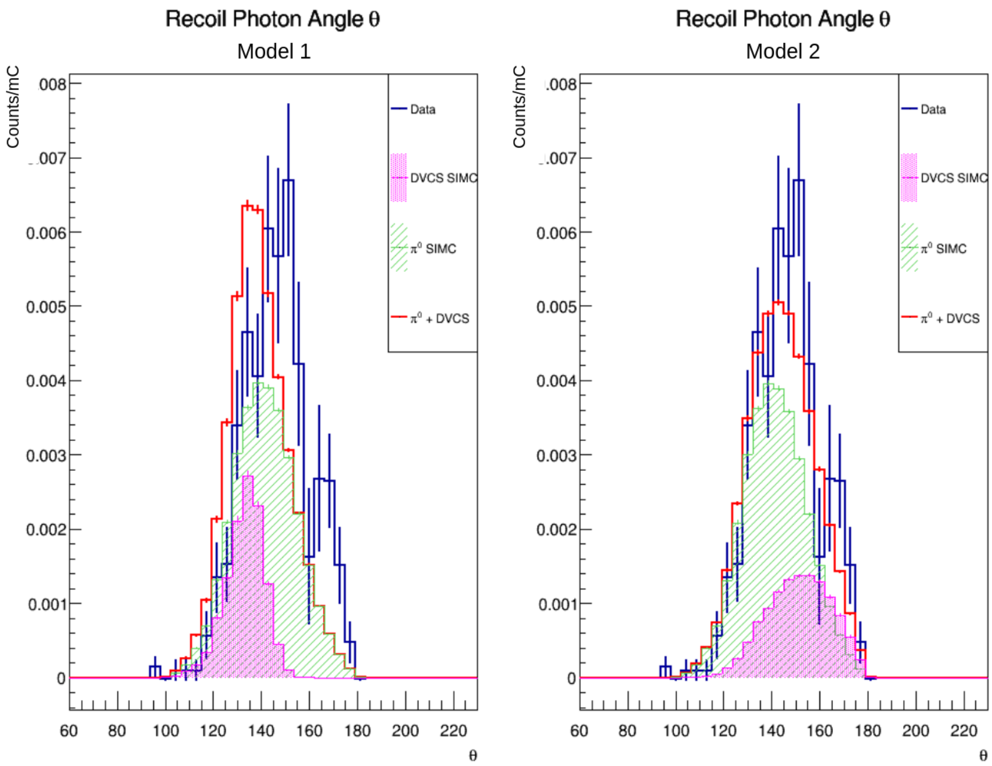

Figure 4.8: DVCS SIMC Model 1 vs Model 2 for angle of recoil photon θ. The DVCS peak from Model 1 (left) resides entirely within the π^0 peak, while the DVCS peak from Model 2 (right) is wider and shifted, and it fills the right shoulder in the data. The difference between the two models is a great source of uncertainty.

4.2 DVCS SIMC Feasibility

In the acceptance cuts, the value of δ of the SHMS is restricted to be from -10% to 20%. δ_{SHMS} is useful to test the feasibility of the DVCS SIMC for datasets with different Q^2 and W, because if there are a significant number of events $< -10\%$ or $> 20\%$, then the data sets should not be studied, since they are not trusted to have been properly reconstructed. δ_{SHMS} is plotted with all acceptance cuts, except for those that limit itself, and with no weights applied due to the issues with the cross-section model (Section 3.1.5). All appropriate SHMS angles with respect to the q vector (left, center, and right) for low and high ϵ were plotted for each dataset. The table summary of all examined datasets is shown in Table 4.2.

The settings with δ_{SHMS} well inside the acceptance range are $Q^2 = 3.0$, $W = 3.14$, and $Q^2 = 5.5$, $W = 3.02$, at both low and high ϵ, and $Q^2 = 2.1$, $W = 2.95$, at low ϵ, which indicates that they are feasible datasets and the DVCS data and SIMC can be trusted. The other settings were not primarily inside the acceptance range, and therefore the data and SIMC cannot be trusted to properly reconstruct the events.

Dataset		SHMS δ Within Acceptance
$Q^2 = 2.1$, $W = 2.95$	low ϵ	✓
	high ϵ	×
$Q^2 = 3.0$, $W = 2.32$	low ϵ	×
	high ϵ	×
$Q^2 = 3.0$, $W = 3.14$	low ϵ	✓
	high ϵ	✓
$Q^2 = 4.4$, $W = 2.74$	low ϵ	×
	high ϵ	×
$Q^2 = 5.5$, $W = 3.02$	low ϵ	✓
	high ϵ	✓

Table 4.2: The feasibility of the DVCS SIMC for various Q^2 and W datasets is determined by examining the variable δ_{SHMS}, and seeing if it falls inside the acceptance range of -10% to 20%. Datasets marked with a ✓ have few to no events outside of the acceptance, while those marked with × have a significant number of events outside of the acceptance. For low ϵ settings, SHMS left and center were examined, and for high ϵ, left, center, and right were examined. The conclusions are the same for the different angles.

The missing mass offset study was attempted for $Q^2 = 3.0$, $W = 3.14$, SHMS center, high ϵ, and $Q^2 = 2.1$, $W = 2.95$, SHMS center, low ϵ, but results were inconclusive, in part due to low statistics. $Q^2 = 5.5$, $W = 3.02$, was not studied at all due to low statistics in the data.

4.3 Rate Estimates

The peak of the missing mass squared plot can be integrated to obtain an estimate for the total number of events that were recorded in the π^0/DVCS region. Furthermore, knowing the beam current, the total events per hour can be computed with simple dimensional analysis. The integral of the raw charge-normalized peak for the setting $Q^2 = 3.0$, $W = 3.14$, SHMS center, low ϵ is 0.03187 counts/mC, and the beam current is 40 uA = 40 uC/s, which estimates a count rate of

$$0.03187 \, \frac{\text{counts}}{1 \text{ mC}} \times \frac{1 \text{ mC}}{1000 \text{ uC}} \times \frac{40 \text{ uC}}{1 \text{ s}} \times \frac{3600 \text{ s}}{1 \text{ h}} = 4.589 \, \frac{\text{counts}}{\text{h}}.$$

The rates were also estimated for $Q^2 = 3.0$, $W = 3.14$, SHMS center, high ϵ, and $Q^2 = 2.1$, $W = 2.95$, SHMS center, low ϵ. Additionally, the rates predicted by the π^0 SIMC are determined using a similar method. The results can be found in Table 4.3.

Setting		**Data Rate (/hr)**	**SIMC Rate (/hr)**
$Q^2 = 3.0$, $W = 3.14$	low ϵ	4.589	11.33
	high ϵ	39.89	110.6
$Q^2 = 2.1$, $W = 2.95$	low ϵ	3.699	4.224

Table 4.3: Rate estimates at different settings. The rates are calculated by integrating the peak in the missing mass squared and using dimensional analysis alongside the charge values and current (constant at 40 uA). The SIMC consistently predicts a rate larger than the data.

4.4 Conclusion

This work investigates the potential evidence for u-channel DVCS in KaonLT data. If found, it would be the first ever measurement, and it would provide more information on baryon number distribution in the proton [10]. The experimental settings with the strongest evidence are at $Q^2 = 3.0$ and $W = 3.14$, with the SHMS at the center angle, and at low ϵ. Settings of $Q^2 = 3.0$, $W = 3.14$, SHMS center, high ϵ, and $Q^2 = 2.1$, $W = 2.95$, SHMS center, low ϵ, were deemed feasible by studying the behaviour of δ_{SHMS} in the DVCS SIMC and thus were briefly examined, but results were inconclusive because of limited statistics in the data.

Events from π^0 DEMP and DVCS were selected using cuts on the various data collected by the spectrometers (Section 3.1) and the missing mass squared (with all of the event selection cuts) was used to scale the π^0 and DVCS SIMC predictions (Section 3.2) to the data. The scaled SIMC predictions were then visually compared to the data for various kinematic variables (Section 4.1). In almost all of the kinematic plots, the DVCS could likely not be resolved from the π^0. This work also examined the different DVCS cross-section models, and compared Model 1 and Model 2 (Section 4.1.1). It was found that DVCS was most different from π^0 in the recoil photon angle with the Model 2 weight (Figure 4.8). Finally, this work provides estimates for the event rate of π^0/DVCS, and it compares the data to what is predicted by the π^0 SIMC (Section 4.3).

4.5 Future Work

This work is a valuable starting point of the investigation into whether or not u-Channel DVCS was measured in KaonLT. It has also brought important things to attention, such as the difference in the two weight models, so that they may be more thoroughly examined. At the moment, there is a huge uncertainty on the DVCS because of this, so future development could lead to a more precise prediction of the DVCS cross-section in the model. This work also examined the feasibility of different settings, which could potentially be useful for future experiments measuring DVCS.

The rate estimates in this work are useful in the run-planning stage of an upcoming experiment that will perform a Q^2 scaling test on the π^0 reaction [11]. The data from that experiment could potentially validate the DVCS signal observed in KaonLT. This work can also help inform experiment design at the upcoming Electron-Ion Collider (EIC), for which there is already interest in measuring u-channel DVCS [12].

Finally, since the settings with the best DVCS signal were found in this work to be $Q^2 = 3.0$, $W = 3.14$, the cross-section of the sum of π^0 and DVCS reaction can be calculated from this data.

References

[1] D. J. Griffiths. Introduction to Elementary Particles (2nd rev. ed.). Wiley (2008).

[2] R. Devenish and A. Cooper-Sarkar, Deep Inelastic Scattering, Oxford University Press (2003).

[3] M. Diehl, Generalized Parton Distributions, Phys. Rep. 388 2 (2003).

[4] J.P. Lansberg, B. Pire, and L. Szymanowski, Backward DVCS and Proton to Photon Transition Distribution Amplitudes, Nucl. Phys. A 782 1 (2007).

[5] A. Usman (PhD Thesis). The Study of Exclusive Pion Electroproduction Reaction from KaonLT Experiment at Jefferson Lab Hall C. *University of Regina* (2025).

[6] W. Li (PhD Thesis). Exclusive Backward-Angle Omega Meson Elecroproduction. *University of Regina* (2017).

[7] C. Tennant et al. Superconducting radio-frequency cavity fault classification using machine learning at Jefferson Laboratory. Phys. Rev. Accel. Beams 23, 114601 (2020).

[8] E.R. Kinney (PowerPoint Slides). The Jefferson Lab Hall C Program: Physics at the Luminosity Frontier. *University of Colorado* (2022). https://indico.mit.edu/event/538/contributions/1509/attachments/562/950/Kinney_HallC_v1%20Ed%20Kinney.pdf

[9] W.B. Li et al, Backward-angle Exclusive pi0 Production above the Resonance Region, Jefferson Lab PAC 48 Experiment Proposal, arXiv:2008.10768 [nucl-ex] (2021).

[10] B. Pire, K. Semenov-Tian-Shansky & L. Szymanowski, Transition distribution amplitudes and hard exclusive reactions with baryon number transfer, Phys. Rep. 940 (2011).

[11] W. Li et al. Short Plan for a u-Channel Scaling Study. E12-20-007 Experiment Internal Document (2025).

[12] Z. Sweger et al, Modeling Backward-Angle (u-channel) Virtual Compton Scattering at an Electron-Ion Collider, Phys. Rev. C 108 055205 (2-23).